RSC Advances

PAPER

View Article Online
View Journal | View Issue

Cite this: *RSC Adv.*, 2018, **8**, 32506

Chemistry of black leaf films synthesised using rail steels and their influence on the low friction mechanism†

Kei Ishizaka,[ab] Stephen R. Lewis,[ac] Deborah Hammond[d] and Roger Lewis*[a]

Received 17th July 2018
Accepted 12th September 2018

DOI: 10.1039/c8ra06080k

rsc.li/rsc-advances

Fallen leaves are the main issues for train operations in the autumn season due to their low friction coefficient (COF), leading to signals being passed dangerously and amended timetables. The main aim of this study was to elucidate the mechanism of low friction due to black leaf films, which are often seen on leaf-contaminated rails. A black material was successfully synthesised in the laboratory with water extracts from sycamore leaves and a plate of R260 rail steel. The black powder made from the extracts of brown leaves (BBP) was identified as the key material of low friction by the pin-on-flat tribological test, giving a COF between 0.08 and 0.14, which was lower than the COF of commercial engine oil (approximately 0.14). X-Ray fluorescence showed that the black material was a mixture of iron and leaf-organics. Laser Raman spectroscopy revealed that graphite-like carbon was likely to be formed on iron oxides. Fourier transform infrared spectroscopy showed that the formation of iron carboxylate was likely in bulk, which possibly transformed into iron oxides on the surface. Moreover, X-ray photoelectron spectroscopy detected a relatively high concentration of phosphates only in BBP. Hence, the low friction is presumably due to graphitic carbon, iron oxides and phosphate compounds in the black leaf films, as well as mechanical separation effects of bulk leaves. This black material could be a product of the Maillard reaction or reaction between iron and organic acids, such as tannic acids.

1. Introduction

Traction between wheels and rails, which is often expressed as "adhesion" in the railway industry, is one of the most critical factors for train control: acceleration and deceleration. The friction coefficient, COF, is required to be at least 0.2 and 0.09 for traction and braking, respectively.[1] However, the rail surface is often contaminated with various sources due to the open environment of railway tracks, and the adhesion condition is sometimes below the required level.

Among various contamination sources, leaves falling on the line in autumn have a significant impact on train operation.[2] They form a black, hard and "Teflon-like" film on the rail, which decreases the traction coefficient to 0.1 or lower when a small amount of water, such as light rain or morning dew, is present.[3,4] The leaf film often causes serious problems in terms of safety and service, such as station overruns,[5] collisions[6] and amended timetables.[7,8] Additionally, the annual loss due to leaf contamination is reported to be £50 million in the United Kingdom[9] and 100 million SEK in Sweden.[10]

Some measures for mitigation are taken to overcome low friction due to leaf contamination. For example, sanding and rail cleaning by high-pressure water jetting are currently used to increase adhesion levels in the autumn.[4] However, they have some drawbacks: high wear rates of both wheels and rails in sanding[11–15] and incomplete removal of leaf films in water-jet cleaning.[1] Moreover, these measures are usually carried out by a cleaning train called RHTT (Rail Head Treatment Train), and the cost associated with RHTTs accounts for half of the total cost, approximately £25 million.[16] For a further reduction in cost, a new prevention method of leaf film formation – rather than mitigation – is necessary.

Recently, many researchers have tried to reveal what leaf films consist of and to clarify the mechanism of low friction conditions, using techniques of chemical analysis. For instance, an infra-red reflection absorption microspectroscopy (IR) analysis suggests that pectin in leaves causes a chemical reaction with rail steels, forming an iron pectate.[17] In the chemical reaction process, the pectin possibly forms a gel by crosslinking with iron ions, and this gel causes low friction due to its high viscosity, forming an elastohydrodynamic lubrication (EHL) film. Another theory is a friction-reducing layer formed on rails

[a]*Department of Mechanical Engineering, The University of Sheffield, Mappin Street, Sheffield S1 3JD, UK. E-mail: roger.lewis@sheffield.ac.uk; Fax: +44(0) 114 222 7890; Tel: +44(0) 114 222 7838*

[b]*East Japan Railway Company, 2-2-2 Yoyogi, Shibuya-ku, Tokyo 151-0053, Japan*

[c]*British Steel, Scunthorpe Rail and Section Mill, Brigg Road, Scunthorpe, DN16 1BP, UK*

[d]*Sheffield Surface Analysis Centre, Department of Chemistry, The University of Sheffield, Dainton Building, Brook Hill, Sheffield S3 7HF, UK*

† Electronic supplementary information (ESI) available. See DOI: 10.1039/c8ra06080k

because of a chemical reaction between leaf-organics and rail steels.[18] Glow Discharge Optical Emission Spectroscopy (GD-OES) reveals that a field rail sample contaminated with leaves contains organic elements, such as carbon, nitrogen and calcium on the surface, but iron oxide exists beneath the surface, forming a mixed layer. This mixed layer is supposed to cause low friction as well.

However, these theories have some drawbacks. For example, carboxylate bands detected during IR analysis do not necessarily derive from pectin; they could be attributed to other materials which have carboxylates in them. In the friction-reducing layer theory, the chemical reaction process has not yet been considered. In spite of the significant progress of these studies, a detailed mechanism of how organics in leaves react with rail steels is still unknown. If this mechanism is clarified, it could lead to a development of innovative methods, which can prevent leaf film formation.

Hence, this study aimed to identify the key materials for low friction due to leaf contamination and to obtain the chemical information of those materials. As a first step, several hypotheses for low friction were developed, such as bulk leaf, adhered leaf film and pectin gel, as reported in.[4] Based on these theories, the candidates of possible substances were narrow-downed, and the identified material was investigated, using several chemical analysis techniques.

2. Methods and materials

2.1 Test samples

Six types of leaf-related samples were examined in this study: leaf powder (LP), leaf extract (LE) and black precipitation powder (BP) for green and brown sycamore leaves, as shown in Fig. 1. Sycamore leaves were chosen as they are recognised as one of the problematic leaves,[1,2,19] and they have been found to cause low friction conditions in previous work.[9,17,20,21] Brown sycamore leaves were collected in Sheffield between November and December 2015. Green leaves were picked from trees at the same site between October and November 2016 and kept in a freezer to minimise decay.

Bulk leaves were chopped by a food processor, and then they were filtered by a strainer, separating small pieces from relatively large pieces. The former was categorised as LP, and the latter was leaf mulch (LM). The typical size of the LP particles was between 15 and 800 μm, measured with an optical microscope.

LE was made by mixing LM with distilled water at a ratio of 1 g of LM to 50 ml of distilled water. After mixing, the mixture was left for one to three days, then it was filtered with filter-paper, removing small particles.

BP was synthesised with LE (typically one day extraction) and a plate made of rail steel (R260). A rail plate was immersed in LEs and left for one to three days, forming black precipitation due to a chemical reaction between iron from the plate and dissolved organics in LEs. Then, the mixture was heated and brought to a boil to accelerate the chemical reaction and evaporate the water. Due to this boiling process, the black precipitation was dried, and they were ground using a pestle and mortar. Typically, the size of the BP particles was between 10 and 100 μm, measured in the same manner as the LP particles. It should be noted that high flash temperatures can be achieved in the wheel/rail contact due to localised slip in the wheel/rail contact.[4] Consecutive wheel passes over a leaf on the

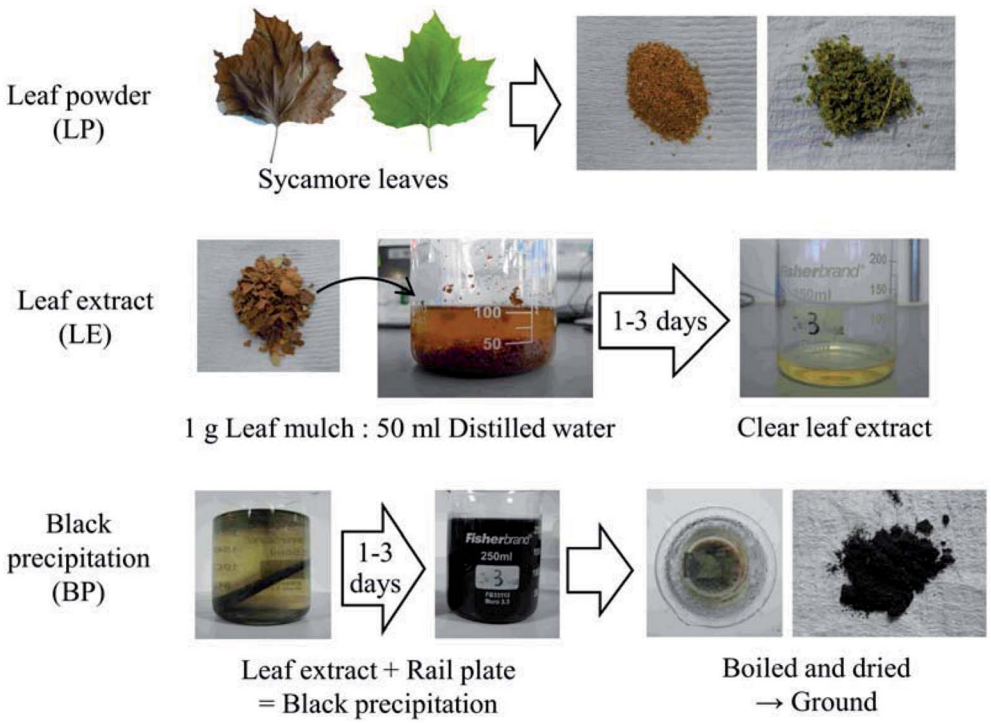

Fig. 1 Preparation of leaf-related samples.

rail would add temperature to the leaf. Thus, this boiling process does not excessively enhance the chemical reaction, as high temperatures are expected in addition to high contact pressures up to 1 GPa.

For some chemical analysis, two types of BP films were analysed: a thin BP film and thick BP film. BP thin films were prepared on a small piece of rail steel, approximately 10 × 10 × 4 mm. They were formed following the procedure of BP formation; however, no heat was applied to the steel piece unlike in the BP formation. This method allows replication of the black material on railway tracks as naturally as possible. BP thick films were formed on the small steel piece, fully following the procedure of BP formation.

It should be noted that BP can be synthesised with leaf extracts of other types of leaves, such as silver birch, oak and ash. Lubricity or chemical properties of BP might depend on the types of leaves; however, only BP derived from sycamore leaves was examined in this study as sycamore leaves have been known to cause low friction in both laboratory experiments and actual train operation. The effects of different types of leaves should be examined in the future.

2.2 Viscosity measurement

Viscosity measurements were performed with a Brookfield DV1 Viscometer. A viscosity value was measured at 100 rpm and 30 °C, with a SC4-18 spindle.

2.3 Friction tests

A basic ball-on-flat test was conducted using the six leaf-related samples, as shown in Fig. 2. This test aimed to investigate the hypotheses for low adhesion: bulk leaf and pectin gel.[4] The LP represents a bulk leaf on the line, and the LE and BP examine the pectin hypothesis. As a reference, three liquid samples were also tested: distilled water, engine oil (Servol 15W-40, Morris lubricant) and pectin 0.1 wt% solution. Pectin powder was purchased from Sigma-Aldrich (product number: P9135, CAS number: 9000-69-5). The concentration of pectin solution was determined by the viscosity value of the LEs.

Table 1 summarises the experimental conditions of friction tests. Specimens were a 5 mm diameter stainless-steel ball and a plate made of R260 rail steel (66 × 25 × 4 mm), which typically had a surface roughness between 0.4 and 0.6 μm Rq. LP and BP were diluted with distilled water, making a 5 weight percent (wt%) solution. LE was directly applied to the rail plate. A Bruker UMT machine was used for the friction tests, following this process; approximately 0.2 ml of sample solution was applied to the fixed rail plate. Then the ball was pressed into the plate with 10 N, giving an average Herzian contact pressure of 1.56 GPa. The ball was reciprocated for six minutes at 0.4 Hz, while the friction coefficient (COF) was measured. The COFs were averaged for every 20 seconds and evaluated. The measurement was repeated at least three times, and the standard deviation was calculated to show the spread in friction values.

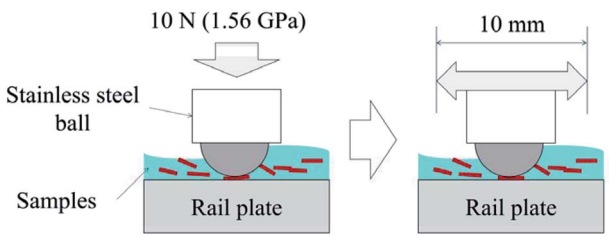

Fig. 2 Experimental procedure of friction tests.

Table 1 Experimental conditions of friction tests

Parameter	Value
Applied force [N]	10
Average Hertzian pressure [GPa]	1.56
Time [seconds]	360
Stroke [mm]	10
Frequency [Hz]	0.4
Sampling frequency [Hz]	100
Top stainless-steel ball diameter [mm]	5
Sample amount [ml]	0.2
Concentration (LP and BP) [wt%]	5

2.4 Characterisation

Several analyses were carried out for mainly BP, but also LE and LP: viscosity measurement, X-Ray Fluorescence (XRF), X-Ray Diffraction (XRD), Laser Raman Spectroscopy (RS), X-Ray Photoelectron Spectroscopy (XPS) and Fourier Transform Infrared spectroscopy (FT-IR). Each technique has its disadvantages or limitations; it was important to combine several methods to establish what material BP is made from. Details of each method are described below.

2.4.1 X-ray fluorescence (XRF). A Fisherscope XAN 250 was used for XRF analysis of BP and LP. The main limitation of this method was incompleteness in detection. In this machine set-up, the elements between aluminium (Al, 13) and uranium (U, 92) are measurable; the light elements between hydrogen (H, 1) and magnesium (Mg, 12) cannot be detected.

2.4.2 X-ray diffraction (XRD). A PANalytical X'Pert^3 Powder was used to obtain XRD data. The data was taken at an angle between 10° and 80°, with a scanning step of 0.01313° and Cu-Kα X-ray source. It should be noted that XRD can only detect material which has a crystal structure. Therefore, no peaks in the acquired data could mean an amorphous structure.

2.4.3 Laser Raman spectroscopy (RS). A Renishaw inVia Raman microscope was used for RS analysis, with BP and BP thin films. The wavelength of the laser was 514.5 nm (green), and the original laser power was set as 20 mW. In all experiments, the objective lens ×50 was used, and the spot size was approximately five μm in diameter. Typically, the spectrum was acquired between 50 and 4000 cm^{-1} with the exposure time of 10 or 20 seconds and five-time accumulation, reducing the laser power to 5 or 10% (approximately one or two mW). A baseline of the acquired spectrum was subtracted, and the noise on the spectrum was removed with WiRE software, making the spectrum flat and smooth. For some spectra, peak fittings were also conducted. As a reference, activated charcoal was also analysed,

which was purchased from Sigma-Aldrich (product number: C9157, CAS number: 7440-44-0).

2.4.4 X-ray photoeletron spectroscopy (XPS). XPS analysis was performed for BP thin and thick films with a Kratos Analytical Axis Supra. The sample piece with BP films was fixed to the stage by a double-sided sticky tape to achieve the electrical isolation. A piece of paper was used to guarantee the insulation between the sample and stage: stage-double sided tape-paper-double sided tape-sample. Due to this structure, the whole sample surface would be uniformly charged-up, and the neutraliser could keep the electrical level constant with low energy electrons. Before a measurement, Ar ion sputtering was conducted to remove thin contamination layer on the top, *i.e.*, a natural oxide layer, with Ar 2000+ clusters at 5 kV for 20 seconds, targeting an area 5 × 5 mm. Then, X-rays were irradiated at 1486.6 eV with an Al source, spotting the area of 300 × 700 μm.

Spectra between 0 and 1200 eV were measured at 160 eV pass energy, 1 eV intervals, and with five minutes of acquisition time. After that, the high-resolution spectrum of each element was collected at 20 eV pass energy and 0.1 eV intervals for 5 to 15 minutes. These acquired spectra were analysed with CasaXPS processing software (Version 2.3.19). Firstly, they were calibrated with carbon 1s peak at 285 eV to cancel a shift due to charging-up. Then, each peak was fitted with appropriate Gaussian–Lorentzian (GL) ratio and full width at half maximum (FWHM) to acquire an accurate value of chemical shift in each peak. Finally, the chemical shift values were compared to data in the references. The measurement was repeated three times or more at different spots.

2.4.5 Fourier transform infrared spectroscopy (FT-IR). A Bruker ALPHA Platinum-ATR was used, and FT-IR spectra were taken for BP and LP, between 400 and 4000 cm^{-1}, scanning 16 times with the resolution of 4 cm^{-1}. The region between 4000 and 1500 cm^{-1} was mainly analysed, as the fingerprint region between 1500 and 600 cm^{-1} usually shows complex absorption patterns and they are relatively difficult to analyse. Additionally, the spectra had a noise between 1900 and 2200 cm^{-1}, which is attributed to the diamond stage of the machine. Hence, assignments to specific molecular bonds in these regions could be inaccurate.

3. Results and discussion

3.1 Viscosity measurement

Table 2 summarises viscosity values of green leaf extract (GLE), brown leaf extract (BLE), distilled water and pectin 0.1 wt% solution. The viscosity values of GLE and BLE were found to be at the same level as distilled water. In contrast, the artificial pectin 0.1 wt% solution exhibited higher value than the LEs. This result indicates that leaf components with high molecular weight are unlikely to dissolve into LEs in terms of viscosity values. If pectin dissolves in LEs as suggested in,[17] a concentration of pectin in LEs could be very low, under 0.1 wt% at least. Or pectin is decomposed from polysaccharide to monomer (a structural unit), such as a galacturonic acid,[22] and it does not affect viscosity values.

Table 2 Viscosity measurements

Extraction time	Viscosity [mPa s]			
	GLE	BLE	Reference	
1 day	1.08	1.08	Distilled water	1.08
2 days	1.05	1.02	Pectin 0.1 wt%	1.62

3.2 Friction tests

3.2.1 Leaf extracts. Fig. 3(a) illustrates the results of friction tests with green leaf extract (GLE) and brown leaf extract (BLE): three days and one day extraction, respectively. Both GLE and BLE showed a medium-low level of friction between 0.2 and 0.25 after six minutes. This range of COF is lower than distilled water and pectin solution, which showed around 0.45 and 0.3, respectively. This result shows that LEs have some impurities which affect friction levels, and they are unlikely to be pectin. Additionally, black material was formed after some tests, showing a good agreement with.[17] However, no black material was found after the tests of pectin 0.1 wt% solution, suggesting that the artificial pectin has nothing to do with the chemical reaction.

Moreover, BLE exhibited low COF for the first 20 seconds, which is almost the same level as the engine oil. However, the friction level gradually increased and settled around 0.25 after six minutes. GLE constantly showed a medium-low level of friction, which is between 0.2 and 0.25. Thereby, no significant difference was observed between GLE and BLE except for the first 60 seconds.

3.2.2 Leaf powder solution. Fig. 3(b) depicts the results of friction tests with green leaf powder (GLP) and brown leaf powder (BLP) 5 wt% solutions. Both GLP and BLP solution exhibited low COF, which is lower than the engine oil up to 60 seconds. They showed medium-low friction level around 0.15 to 0.2 after six minutes, which is much lower than the level of distilled water.

This result suggests that LP possibly prevents the metal–metal contact between the ball and plate, acting as a solid lubricant. As the experiment proceeded, the LP solution was gradually removed from the contact area. Subsequently, the friction level increased due to less solid lubrication effects of LP. Instead of LP, LE then affected the friction condition more, and the COF became around 0.2 because of the mixed lubrication of LP and LE.

It should be noted that both GLP and BLP became black during the tests; the chemical reaction quickly occurred on the surface of LP, where the concentration of impurities could be high.

3.2.3 Black precipitation powder solution. Fig. 3(c) exhibits the results of friction tests with black precipitation powder formed in green leaf extracts (GBP) and black precipitation powder formed in brown leaf extracts (BBP). Surprisingly, BBP solution showed extremely low friction, which is lower than the engine oil up to 160 seconds and at the same level afterwards. In contrast, GBP solution showed a stable COF around 0.2,

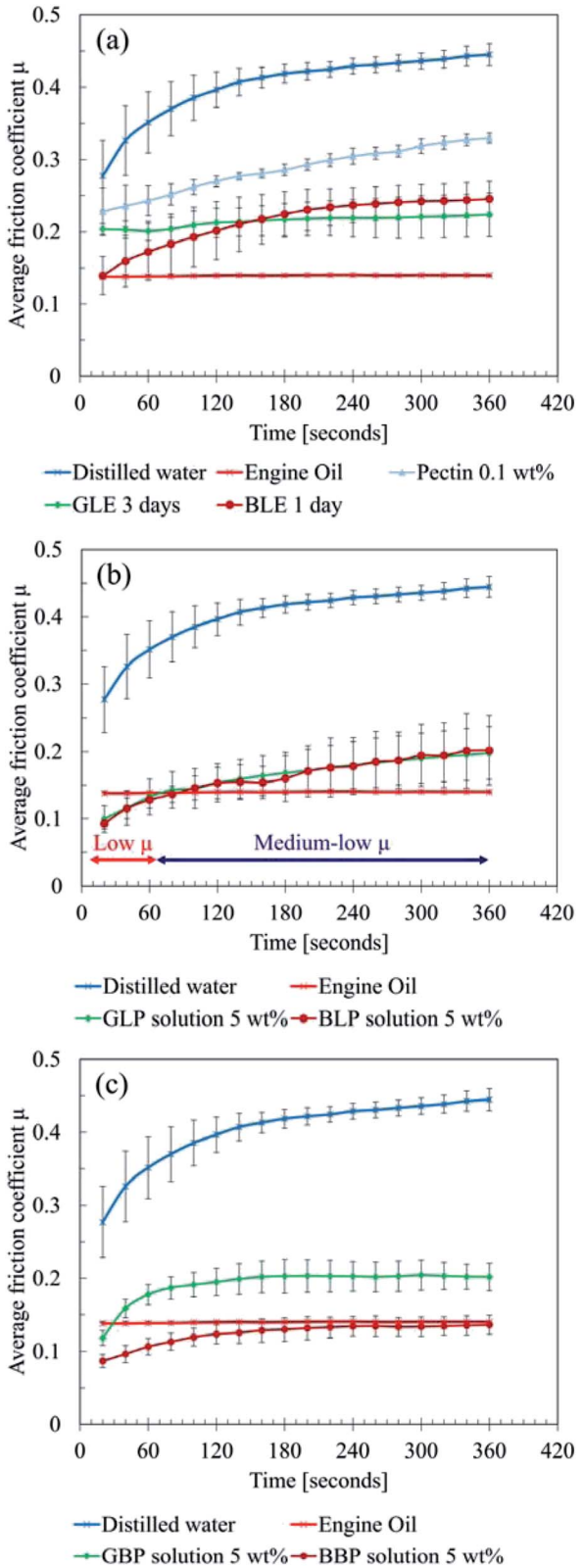

Fig. 3 Results of friction tests (a) leaf extracts, (b) leaf powder solution, (c) black precipitation powder solution.

although it exhibited very low friction for the initial 20 seconds. This result shows that BBP is a key material for low friction. Moreover, the difference between GBP and BBP in terms of materials could identify a substance which is directly relevant to low friction.

Overall, the friction tests showed three main findings:

- Bulk leaf powder acts as a solid lubricant if it is in the contact area.
- Water-soluble organics in sycamore leaves do not lower the COFs dramatically, although they help the formation of black materials.
- The black material is mainly responsible for low friction.

Thus, the "bulk leaf" hypothesis in[4] is likely to be true as the low COFs were confirmed. However, the hypothesis "pectin gel" could be untrue in terms of pectin as a key material, because pectin is unlikely to be in LEs as a thickening agent and to cause the chemical reaction. Rather than a long pectin chain, there could be decomposed pectin molecule or other organics in LEs, and they can form a black material which finally causes friction.

3.3 Material analysis

3.3.1 X-ray fluorescence (XRF). Fig. S1† depicts the XRF results of GLP, GBP, BLP and BBP. Both GLP and BLP contained a relatively large amount of calcium (Ca) and potassium (K), as well as a small amount of chlorine (Cl), manganese (Mn) and iron (Fe). In contrast, GBP and BBP were found to contain mainly Fe, followed by K, Ca, Cl and Mn. This result shows that Fe ion dissolves into LEs from rail plates, and it causes the chemical reaction with leaf organics in LEs. The dissolved Fe ion presumably reacts with various ions and molecules in LEs, including K, Ca and Cl ions.

It should be noted that the number of counts cannot be directly compared to each other, because the amount of sample powder was not accurately controlled. Thereby, the counts ought to be taken as reference.

3.3.2 X-ray diffraction (XRD). Fig. 4 illustrates the XRD data of GBP and BBP. BBP exhibited several sharp peaks, indicating that some crystal materials were present. In contrast, GBP did not show any peaks, suggesting no crystal structure was in the sample. Table S1† shows the assignments of the peaks in BBP. The assignments were conducted by searching in the database (Powder Diffraction File provided by the International Centre for Diffraction Data: PDF-4). It was found that these XRD patterns of BBP derived from potassium chloride (KCl: strong peaks) and calcium sulphate ($CaSO_4$: relatively weak peaks), although the small two peaks at 20.7 and 31.05 were not identified. Unexpectedly, iron oxides were not detected, suggesting that the iron detected in XRF analysis has an amorphous structure. It should be noted that amorphous KCl and $CaSO_4$ could be present in GBP, as Cl, K and Ca were detected in GBP by XRF analysis.

3.3.3 Laser Raman spectroscopy (RS). Fig. 5 exhibits the acquired Raman spectra of GBP, BBP and activated charcoal, and their peak fittings are shown in Fig. S2.† Both GBP and BBP showed similar peaks, which are around 1350 cm^{-1} (shoulder, small) and 1570 cm^{-1} (strong), respectively. They are typical features of amorphous carbon,[23] called disordered band (D) and graphitic band (G), respectively.[24,25] The broad peak around 2850 cm^{-1} was assigned to amorphous carbon as well,[24]

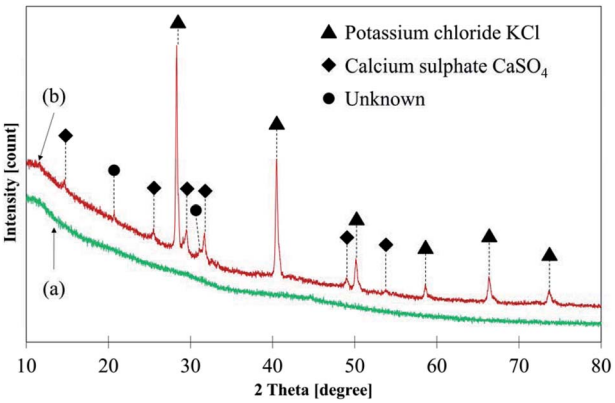

Fig. 4 XRD results: (a) GBP, (b) BBP.

although these peaks in GBP and BBP were not as clear as the activated charcoal. The small and broad peak around 600 cm^{-1} in BBP could be a mixture of magnetite (Fe_3O_4) and hematite (α-Fe_2O_3), which has a shift of 533.6 cm^{-1} and 611.9 cm^{-1}, respectively.[26] The overlapping band around 1430 cm^{-1} was difficult to be assigned; it could be carboxylate ions (COO^-) in carboxylic acid salts,[27] taking into account the result of FT-IR analysis described later in Section 3.3.5.

In general, an intensity ratio of D and G band (I_D/I_G) can be used to evaluate the degree of graphitisation;[24,25,28,29] the ratios were around 0.77, 0.83 and 1.09 for the GBP, BBP and activated charcoal, respectively. These relatively low ratios in GBP and BBP suggest that their carbon materials have a less disordered structure, possibly forming a mixed structure of sp^2 and sp^3 carbon according to the definition in.[30] Hence, both GBP and BBP are likely to have partially graphite-like carbon in them.

This graphite-like carbon could be one of the reasons why low friction happened during the friction test. Furthermore, a sugar-derived carbon, which is often studied as a material of electrodes, has been reported to have a more graphitic structure than amorphous carbon, *e.g.* carbon black.[25,28] Hence, the Raman spectra also indicate that GBP and BBP might derive from dissolved sugars in LEs, which are highly likely in water-extract of plants, such as green tea.[31]

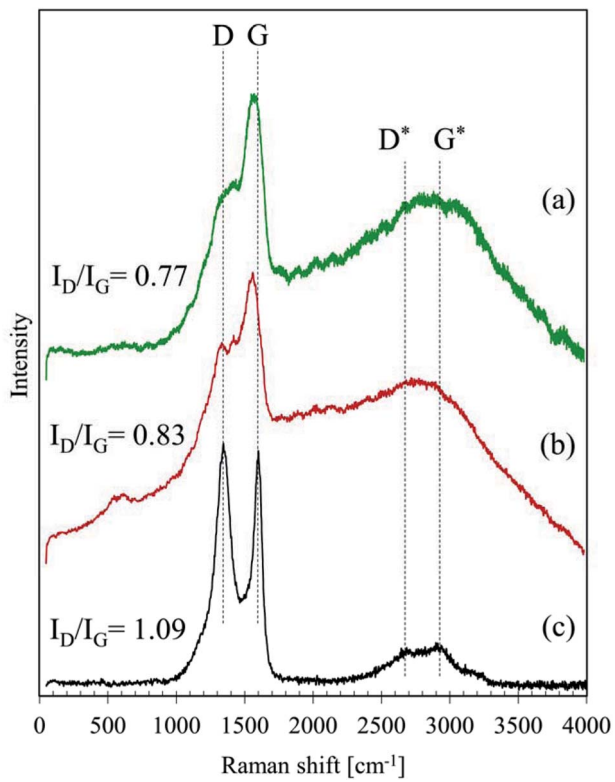

Fig. 5 Raman spectra: (a) GBP, (b) BBP, (c) activated charcoal.

Fig. 6 depicts the Raman spectra of GBP and BBP thin films formed on a small piece of rail steel without boiling. For these samples, two different levels of laser power were tested: 1 and 2 mW. Both GBP and BBP samples showed sharp peaks with the 2 mW laser. In contrast, these clear peaks were not seen in the spectra measured with the 1 mW laser power except D and G bands of carbon. Table 3 summarises the observed Raman shifts and their assignments. The relatively sharp peaks around 220, 290, 400, 600 and 1310 cm^{-1} were assigned to α-Fe_2O_3. The broad and small peak around 650 cm^{-1} could belong to a mixture of Fe_3O_4 and FeO (wüstite), and the broad but the high peak around 1560 cm^{-1} was assigned to amorphous carbon. The difference between the measured and reference values could be attributed to the different laser power since the Raman shifts of peaks move to lower wavenumbers when higher laser power is used in the case of iron oxides.[26]

The broad peak at 650 cm^{-1} in the spectra measured with 1 mW laser indicates that Fe_3O_4 initially exists in the samples; FeO is often seen in the transformation process from Fe_3O_4 to other types of iron oxides, which could be α-Fe_2O_3 in this case.[26] This transition happens if the laser power is intense enough to cause decomposition of Fe_3O_4. Therefore, these peaks seem to originate from Fe_3O_4.

In RS, the sample surface may be degraded if the laser power is too high,[33] and heat induced by the laser affects measurements.[34] In fact, the laser with high power, such as 10 mW, burned the surface of BP during trials. In Fig. 6, it seems that the 1 mW laser gives no damage, but the 2 mW laser does, and it possibly burns the surface carbon layer and exposes the iron oxides underneath the surface layer. The detected peaks of iron oxides do not derive from the rail plate since the depth penetration of graphite is approximately 50 nm.[23] Thus, the Raman spectra in Fig. 5 and 6 predict a structure of GBP and BBP; Fe_3O_4 or a mixture of α-Fe_2O_3, Fe_3O_4 and FeO becomes a core, and a thin amorphous carbon layer grows on the surface of the iron oxide, which is partially graphitised and might be a sugar-derived carbon formed with sugars in LEs.

3.3.4 X-ray photoelectron spectroscopy. Fig. S3† shows the XPS spectra of GBP thick film and GBP thin film, which were formed with and without heat treatment, respectively. In the same manner, Fig. S4† depicts the XPS spectra of BBP thick film and BBP thin film. Both GBP and BBP films were found to contain various elements, such as carbon, oxygen and iron, showing a good agreement with the previous study[18] and the results of XRF and XRD. Some elements, *e.g.* calcium and potassium, were only seen in thick film samples, indicating that the heat treatment affects the chemical reaction for the

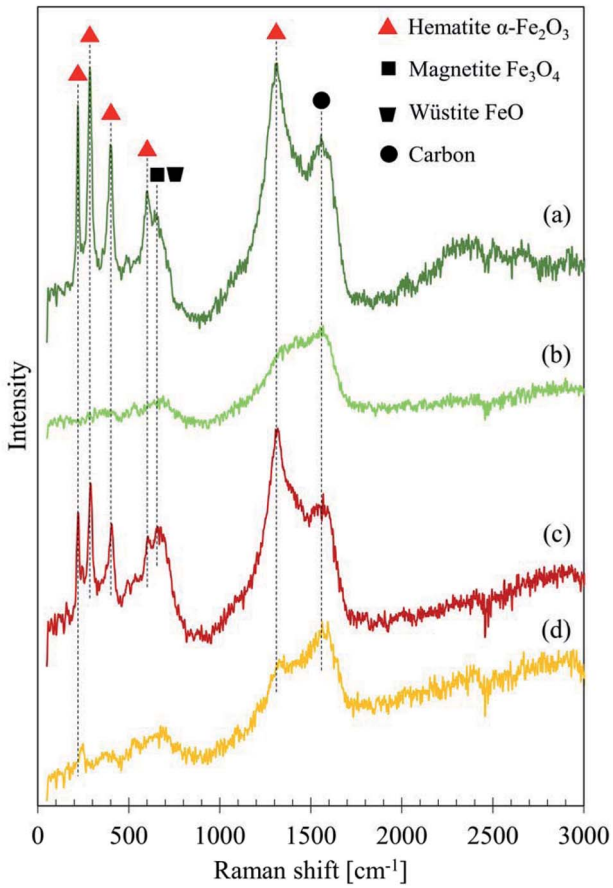

Fig. 6 Raman spectra of GBP and BBP thin films measured with different laser power: (a) GBP 2 mW, (b) GBP 1 mW, (c) BBP 2 mW, (d) BBP 1 mW.

formation of compounds which contain calcium, sulphur, potassium, magnesium, chlorine and silicon.

Table 4 summarises the chemical composition of each element shown in average atomic percent (at%) with the standard deviation. It was revealed that carbon and oxygen accounted for approximately 90 at% in both thick and thin films, possibly forming an organic layer on the surface. Iron was also present in GBP and BBP thin films, accounting for 3–7 at%. However, less or no iron was observed in GBP and BBP thick films, showing that the heat treatment enhanced the chemical reaction which formed the organic layer. This change in the iron composition supports the prediction of a structure: organic layer (carbon layer) on an iron oxide core described in Section 3.3.3. It should be noted that the concentration of sodium was not taken into account due to the lack of the detection in the primary region: Na 1s at 1071.8 eV.

Fig. 7 illustrates C 1s high-resolution spectra and curve fittings of thin and thick films of GBP and BBP. In the same manner, O 1s and Fe 2p high-resolution spectra and curve fittings are shown in Fig. 8 and 9, respectively. Chemical shifts of each element were obtained with these zoomed-in spectra. Table 5 summarises the chemical shifts in binding energies (B.E) and the assignments of GBP samples, and Table 6 does for BBP samples. It should be noted that high-resolution spectra of potassium (K 2p) were not acquired since K 2p has a narrow range of chemical shifts, and they are difficult to interpret accurately.[35,36] Besides, chlorine (Cl 2p) was measured only one time because XRD analysis revealed that KCl was present in BBP.

C 1s was found to contain four components, and their chemical shifts were not dramatically changed after the heat treatment for both GBP and BBP as shown in Tables 5 and 6. Carbon in GBP and BBP seems to be pure carbon (approximately 50 at%), and oxygen-bonded carbon (C–O, C=O and COO). This complex structure is often seen in graphene oxide; it is generally obtained by oxidising graphite particles,[41,47] although observed C 1s did not contain clear sp^2 at 284 eV.[35]

O 1s showed a complex structure as well; GBP thin film contained five components, and BBP thin film did three components, respectively. It should be noted that five components in O 1s were also seen in BBP thin film; however, they were observed only one time and thus classified as a reference value. As shown in Fig. 8, the heating process affected the chemical conditions in O 1s; the component at 530.1–530.6 eV vanished in GBP and BBP thick films. This disappearance means that metal oxides, which are highly likely to be iron oxides, are buried in the organic layer due to the accelerated chemical reaction by the heat treatment. This result also supports the idea of the structure described above.

Another suggestion from the chemical shifts around 534.5 eV is that there could be oxidised graphene (GO). This large chemical shift (+3.5 eV) is unusual for O 1s, and thereby,

Table 3 Raman shifts and assignments of GBP and BBP thin films

GBP 2 mW Raman shift cm^{-1}	BBP 2 mW Raman shift cm^{-1}	Assignment	Reference	
220	222	α-Fe_2O_3	226.7	26
286	290	α-Fe_2O_3	292.5	26
			299.3	
398	406	α-Fe_2O_3	410.9	26 and 32
602	606	α-Fe_2O_3	611.9	26
642	651	FeO	652	26
	662	Fe_3O_4	662.7	32
1305	1317	α-Fe_2O_3	1320	26 and 32
1556	1567	Amorphous carbon	1575	23
		Sugar-derived carbon	1580	25

Table 4 The average chemical compositions of GBP and BBP films in atomic percent

Atomic%	C	O	Fe	N	Mg	P	Mn	Ca	S	K	Cl	Si
Thick GBP	59.3 ± 1.3	35.3 ± 0.9	0.8 ± 0.1	0.7 ± 0.1	—	0.2 ± 0.1	—	1.4 ± 0.1	0.6 ± 0.1	1.0 ± 0.3	0.4 ± 0.1	0.4 ± 0.1
Thin GBP	55.1 ± 2.0	35.0 ± 0.8	7.2 ± 0.8	1.8 ± 0.3	—	0.5 ± 0.2	0.5 ± 0.2	—	—	—	—	—
Thick BBP	55.2 ± 1.1	31.7 ± 2.2	—	1.4 ± 0.1	1.5 ± 0.2	1.2 ± 0.1	—	1.8 ± 0.1	1.0 ± 0.3	2.2 ± 1.2	4.0 ± 1.4	—
Thin BBP	63.3 ± 0.3	28.8 ± 0.7	3.4 ± 0.4	2.8 ± 0.3	—	0.8 ± 0.3	0.2 ± 0.1	0.7 ± 0.1	—	—	—	—

the assignment is difficult.[35,36,39] However, GO has been reported to exhibit a large chemical shift around 534–534.5 eV, and this chemical shift is attributed to water contamination[40,41] or oligomer of vinylene carbonate on a graphene surface.[42] Considering that the surface carbon seems to be partially graphitic, the small component peaked around 534.5 eV might come from the oxidised or water-contaminated graphene.

As shown in Fig. 9, both GBP and BBP thin films contained subtle satellite peaks of Fe $2p_{3/2}$ and Fe $2p_{1/2}$, and thus Fe^{3+} (α-Fe_2O_3) is likely to be present.[43] In contrast, the satellite peak in GBP thick film was relatively intense and overlapped with Fe $2p_{3/2}$ and $2p_{1/2}$. The chemical shifts were around 710.2 eV (Fe $2p_{3/2}$) and 714 eV (Fe $2p_{3/2}$ satellite), and this satellite peak should come from Fe^{2+} high spin compound.[35,43,44] In terms of the chemical shifts in Fe $2p_{3/2}$, Fe^{3+} is highly likely, possibly forming magnetite.[43] On the other hand, the intense satellite peak is often seen in FeO[35,43] and iron-ligands.[44] As RS suggests the presence of FeO, there could be a mixture of Fe_3O_4 and FeO on the surface of the thick GBP film. Thick BBP film exhibited no iron on its surface, suggesting that the iron is covered with organic layers. This is a clear difference between the GBP and BBP thick films.

The chemical shift of N 1s shows that organic matrix (C–NH_2) is likely in both GBP and BBP rather than nitrites or nitrates.[35,36] Phosphorus is likely to exist as a metal phosphate, possibly bonding to calcium or iron. The concentration of phosphorus is relatively higher in thick BBP film than the other film, and it could be the reason why only BBP showed lower friction than GBP. Calcium, sulfur, potassium and chloride were mainly assigned to $CaSO_4$ and KCl respectively, as they were detected in the XRD analysis of BBP. Magnesium, silicon and manganese do not seem to play an important role in the chemical reaction since they were occasionally detected, and their concentrations were small.

3.3.5 Fourier transform infrared spectroscopy. Fig. 10 shows the FT-IR spectra of GBP and BBP with the original GLP

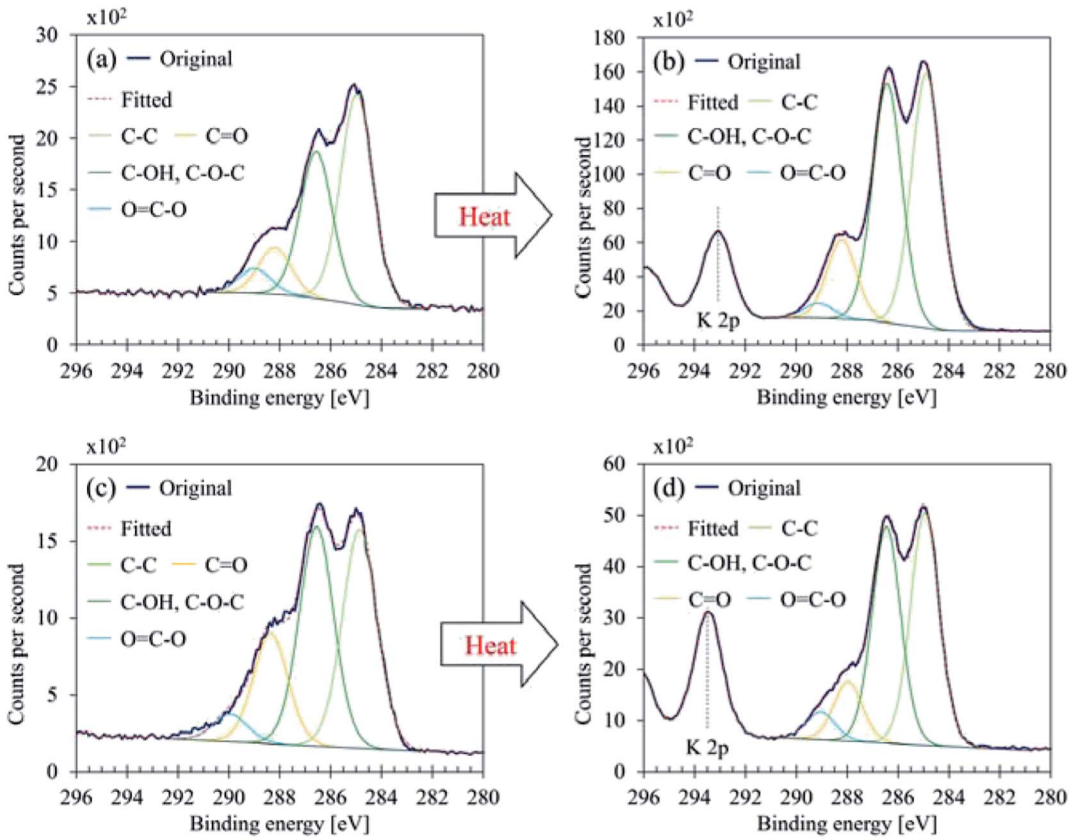

Fig. 7 C 1s curve fittings (a) GBP thin film, (b) GBP thick film, (c) BBP thin film, (d) BBP thick film.

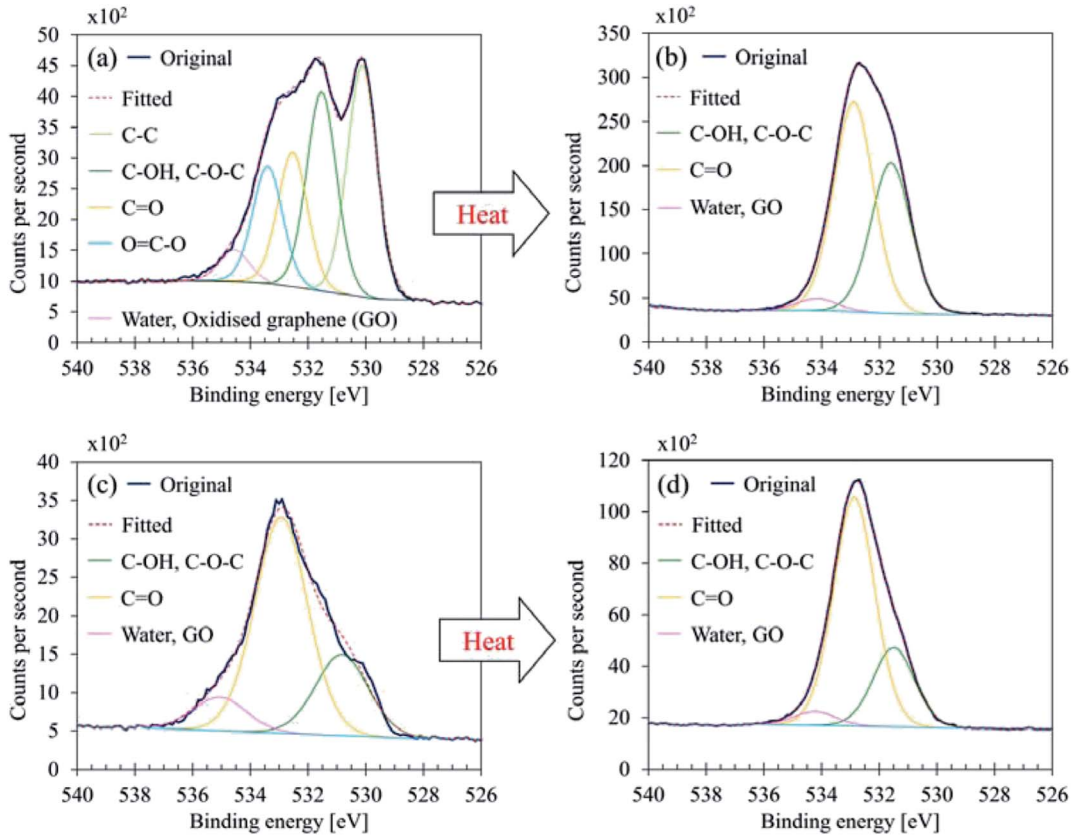

Fig. 8 O 1s curve fittings (a) GBP thin film, (b) GBP thick film, (c) BBP thin film, (d) BBP thick film.

and BLP spectra for comparison. Both GBP and BBP exhibited a similar absorbance: around 3250, 2930, 1600, 1400, and 1100 cm^{-1}. In contrast, the GLP and BLP showed more complex absorption with peaks around 3260, 2920, 2850, 1610, and 1030 cm^{-1}. These absorption bands were assigned as follows: OH stretching at 3260 cm^{-1}, CH stretching at 2920 and 2850 cm^{-1}, C=O double bonds around 1610 cm^{-1}, and C–O stretching around 1030 cm^{-1}, although some small peaks were unable to be assigned. The comparison between BP and LP shows that the BP is different from raw leaves, *e.g.* less clear CH stretching or another peak of C=O.

The assignment of each absorbance in GBP and BBP is shown in Table 7, referring to the literature.[17,27,48–50] The absorption around 3250 cm^{-1} is attributed to OH, which could form both types of hydrogen bonds: inter- or intra-molecular hydrogen bonds. The weak peak at 2930 cm^{-1} presumably comes from saturated CH bonds because unsaturated and aromatic CH frequencies usually are slightly over 3000 cm^{-1} and two sharp peaks should be observed in the case of methyl or methylene groups. In the same manner, NH stretching mode is unlikely because it shows relatively sharp peaks around 3500–3300 cm^{-1}.

Due to the unlikely presence of aromatic CH bonds, two absorbances around 1600 and 1400 cm^{-1} were assigned to carboxylate ions (COO^-), which usually show doublet peaks at 1610–1550 (asymmetric) and 1420–1300 cm^{-1} (symmetric).[17,27,48] C=O double bonds in esters or ketones could be possible in this region, which should appear around 1740 and 1710 cm^{-1}, respectively.[48] However, the significant shifts of the observed absorptions to lower wavenumbers show that they derived from carboxylate ions rather than esters and ketones. N=O double bonds are possible in this region; however, they are unlikely due to the small atomic concentration of nitrogen and the chemical shift found in the XPS analysis (Section 3.3.4).

The band around 1030 cm^{-1} should be CO stretching mode which comes from various organics in GBP and BBP. Further analysis and assignment were not conducted for this CO bond since the region below 1500 cm^{-1} is not diagnostically useful.[48]

As XPS analysis confirmed the presence of iron, iron-carboxylic salts might be formed in GBP and BBP. Fe ions can form a chelate (ligand) structure with some carboxylates, such as oxalate (ferric oxalate) and acetate (ferric acetate).[51,52] Synthesised metal carboxylates exhibit COO^- absorption around 1510–1590 cm^{-1} for asymmetric mode and 1400–1430 cm^{-1} for symmetric mode,[50] which roughly corresponds to the observed values in GBP and BBP. Hence, the observed COO^- in the FT-IR analysis possibly derive from iron carboxylates in BP.

RS and XPS analyses suggest that iron oxides are likely rather than iron carboxylate. However, the thermal energy by laser irradiation in RS could induce the transition of iron carboxylate to iron oxides in this study. Moreover, XPS reflects only properties of the surface up to 10 nm, and the chemical shifts of ferric oxalates in XPS show approximately the same values as

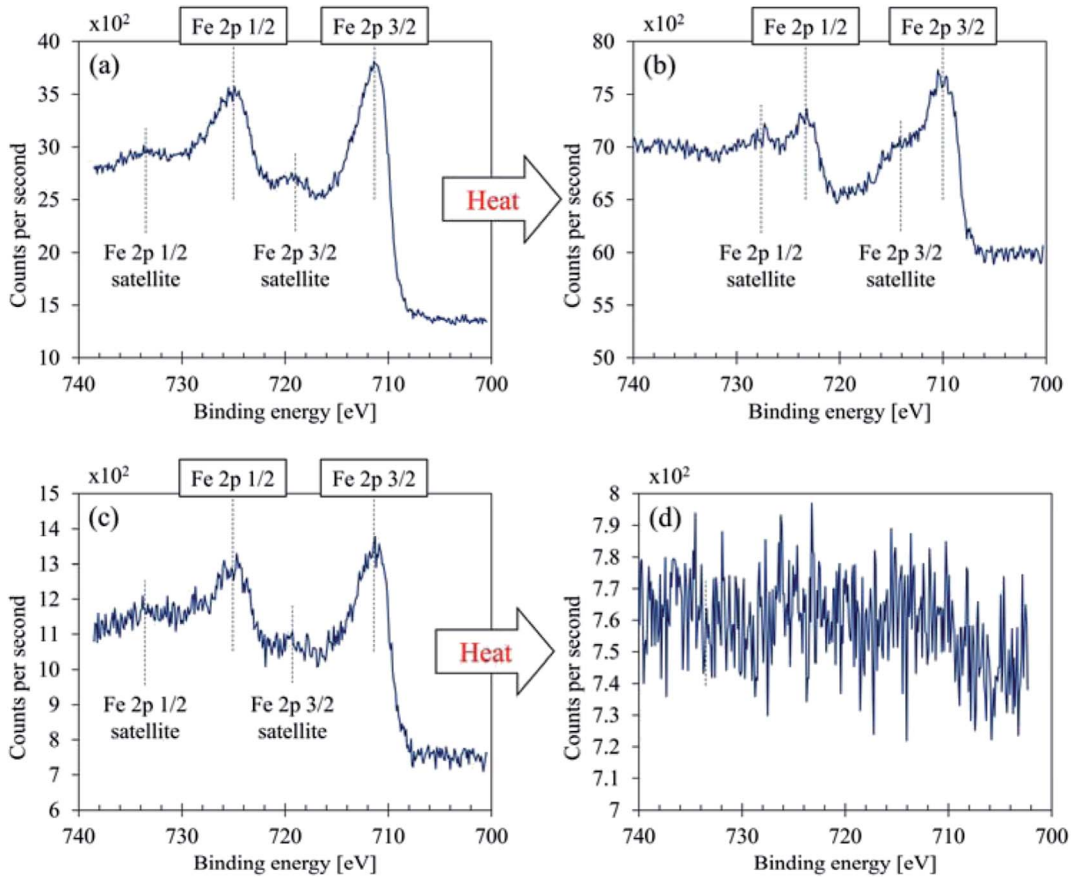

Fig. 9 Fe 2p curve fittings (a) GBP thin film, (b) GBP thick film, (c) BBP thin film, (d) BBP thick film.

iron oxides.[53] In addition, the intense Fe^{2+} satellite might derive from ligand structures, and XRD analysis did not detect crystal iron oxides. Considering all the information from RS, XPS and FT-IR analyses, it can be concluded that the GBP and BBP contain both iron carboxylates and iron oxides; iron carboxylates are predominant in the bulk black material and iron oxides are on the surface. The iron carboxylates are likely to be formed with dissolved Fe ions and carboxylic acids in LEs, then some of them transform to iron oxides due to further oxidisation, especially on the surface.

Table 5 Binding energy (B.E) and assignments of GBP films[a]

Element	Thick GBP B.E	Chemical bonds, expected material	Thin GBP B.E	Chemical bonds, expected material	Reference
P $2p_{3/2}$	—	—	134.1 ± 0.1	Metal phosphate	36 and 37
S $2p_{3/2}$	168.7 ± 0.1	Metal sulphate, $CaSO_4$	—	—	35 and 36
(Cl $2p_{3/2}$)	198.2 ± 0.0	Metal chloride, KCl	—	—	35
C 1s	285.0 ± 0.1	C–C	285.0 ± 0.1	C–C	35, 36 and 38
	286.5 ± 0.1	C–OH, C–O–C	286.6 ± 0.1	C–OH, C–O–C	36, 38 and 39
	288.3 ± 0.0	C═O	288.2 ± 0.2	C═O	36 and 38
	289.1 ± 0.1	O═C–O	289.3 ± 0.4	O═C–O	35, 36 and 38
Ca $2p_{3/2}$	347.6 ± 0.1	$CaSO_4$	—	—	36
N 1s	400.1 ± 0.0	Organic matrix, C–NH_2	400.4 ± 0.0	Organic matrix, C–NH_2	35 and 36
O 1s	—	—	530.1 ± 0.1	Metal oxides, Fe_2O_3	35 and 36
	531.5 ± 0.1	Organic C–O	531.5 ± 0.1	Organic C–O	35
	532.9 ± 0.1	Organic C═O	532.5 ± 0.0	Organic C═O, O═C–O	35 and 39
	—	—	533.4 ± 0.0	O═C–O	39
	534.4 ± 0.2	Water, oxidised graphene	534.5 ± 0.0	Water, oxidised graphene	40–42
Mn $2p_{3/2}$	—	—	641.8 ± 0.2	Mn with O	36
Fe $2p_{3/2}$	710.2 ± 0.3	Iron oxides, Fe^{2+} and Fe^{3+}	711.2 ± 0.1	Iron oxides, Fe^{3+}	35, 36, 43 and 44
(Fe $2p_{1/2}$)	723.6 ± 0.2		724.8 ± 0.2		

[a] Bracket means a reference value: measured only one time or not useful for the determination.

Table 6 Binding energy (B.E) and assignments of BBP films[a]

Element	Thick BBP B.E	Chemical bonds, expected material	Thin BBP B.E	Chemical bonds, expected material	Reference
Mg 2 s	89.3 ± 0.1	$MgSO_4 \cdot MgO$	—	—	45
P $2p_{3/2}$	133.2 ± 0.1	Metal phosphate, ex. $CaHPO_4$	133.7 ± 0.2	Metal phosphate, ex. $FePO_4$	35, 37 and 46
S $2p_{3/2}$	169.0 ± 0.2	Metal sulphate, $CaSO_4 \cdot MgSO_4$	—	—	35 and 36
(Cl $2p_{3/2}$)	198.4	Metal chloride, KCl	—	—	35
C 1s	284.9 ± 0.0	C–C	284.9 ± 0.1	C–C	35, 36 and 38
	286.5 ± 0.0	C–OH, C–O–C	286.5 ± 0.1	C–OH, C–O–C	36, 38 and 39
	288.0 ± 0.0	C═O	288.3 ± 0.3	C═O	36 and 38
	289.1 ± 0.1	O═C–O	289.8 ± 0.5	O═C–O	35, 36 and 38
Ca $2p_{3/2}$	347.6 ± 0.1	$CaSO_4$	347.7 ± 0.1	$CaSO_4$	36
N 1s	400.1 ± 0.0	Organic matrix, C–NH_2	400.3 ± 0.1	Organic matrix, C–NH_2	35 and 36
O 1s	—	—	530.6 ± 0.3	Metal oxides, Fe_2O_3	35 and 36
	531.5 ± 0.1	Organic C–O	(531.7)	Organic C–O	35
	532.8 ± 0.0	Organic C═O	532.9 ± 0.1	Organic C═O	35
	534.4 ± 0.3	Water, oxidised graphene	(534.1)	Water, oxidised graphene	40–42
	—	—	535.1 ± 0.2	Water, Na KLL	35 and 45
Mn $2p_{3/2}$	—	—	641.8 ± 0.1	Mn with O	36
Fe $2p_{3/2}$	—	—	711.2 ± 0.1	Iron oxides, Fe^{3+}	35, 36, 43 and 44
(Fe $2p_{1/2}$)	—	—	724.8 ± 0.2		

[a] Bracket means a reference value: measured only one time or not useful for the determination.

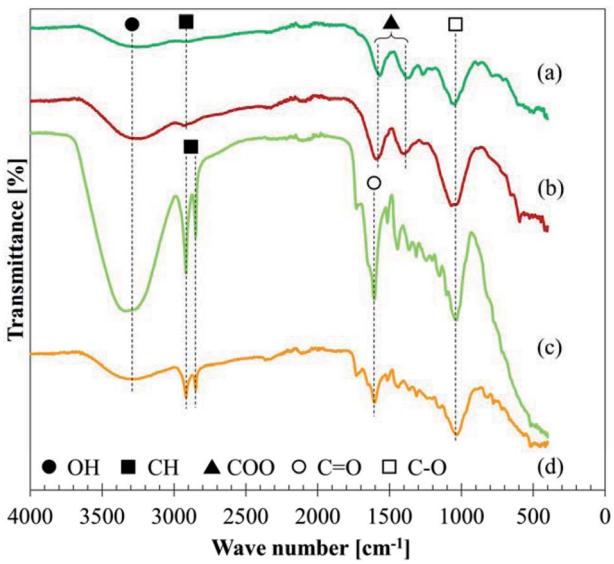

Fig. 10 FT-IR spectra: (a) GBP, (b) BBP, (c) GLP, (d) BLP.

4. Discussion

In this paper, tribological tests were performed as well as material analyses of the black precipitation. Consequently, it was revealed that the black precipitation was the primary material of low friction and it consisted of iron and organics after the chemical reaction process. Considering all the results, the low friction mechanism should be discussed in this section, as well as the chemical reaction process for the formation of black precipitation.

4.1 Low adhesion mechanism

As described in Section 3.2, BP was identified as the main leaf-lubricant for low friction, as well as solid leaf powder, although solid leaves seem to have a limited effect. Table S2† summarises the main findings in the material analyses. In terms of tribology, three of them are very important: graphitic carbon, iron oxides and phosphate compounds.

Fig. 11 shows a schematic diagram of the low friction mechanism due to leaves on the line. Low friction conditions seem to be caused by four factors: graphitic carbon, solid leaf, iron oxide and phosphate compound. Graphite has been recognised as a solid lubricant and widely used.[54] Although the BP does not have a perfect graphite structure, it should be partially graphitised and can contribute to low friction conditions. Solid leaves can reduce the friction level when they are present in the contact area, preventing contact between wheels and rails. Iron oxides are also well-known for their lubricity in the wheel/rail

Table 7 Assignment of each infrared band in GBP and BBP

Assignment	Possible conditions	GBP absorption cm^{-1}	BBP absorption cm^{-1}	Reference
OH stretch	Inter- or intra-molecular H bonds	3280	3232	48
CH stretch	Saturated CH	2934	2938	48
COO^- ion	Chelate structure with metal ions			17, 27 and 48–50
Asymmetric		1570	1593	
Symmetric		1379	1398	
C═O stretch				
CO stretch	Any organics	1046	1071	17 and 48

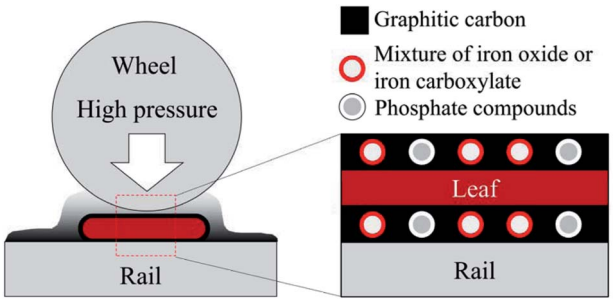

Fig. 11 Schematic figure of low friction mechanism due to leaves.

contact,[4,32] although the mixture of iron oxides and iron carboxylates could be present in the BP. Phosphate compounds are one of the typical anti-wear additives for lubricating oils, such as zinc dialkyl-dithiophosphate (ZDDP). In particular, iron phosphate films formed on steels have been reported to protect the iron surface and reduce wear,[55] and its detailed mechanism has been explained.[56] Furthermore, if the phosphate in BP forms a phospholipid, it dramatically decreases the friction levels in wet conditions.[57] Due to the low concentration of these materials as described in Section 3.3.4, the graphite-like carbon should be the primary cause, followed by bulk leaves and iron oxides, and the phosphate compounds might have a limited effect on low friction.

The synthesised black material was found to contain potassium chloride (KCl) and calcium sulphate ($CaSO_4$), and they might be lubricants as well. However, the reported COF of KCl thin films is not significantly low, around 0.27.[58] Additionally, $CaSO_4$ has a low COF between 0.15 and 0.2 at high temperature (500 or 600 °C), but it is generally brittle at room temperature and does not work as a lubricant.[59,60] Thereby, KCl and $CaSO_4$ in the synthesised black powder are unlikely to be a lubricant. They might have been formed in BBP for a number of reasons, *e.g.* a higher concentration of K^+, Cl^-, Ca^{2+} and SO_4^{2-} ions in BLEs than GLEs. Chemical analysis should be carried out for leaf extracts, *i.e.* ion chromatography and inductivity coupled plasma mass spectroscopy.

As described in Section 1, two main hypotheses have been suggested to explain the main cause of low friction due to leaf contamination: iron pectate[17] and friction reducing oxide layer.[18] However, they were found to be unlikely according to the analyses conducted in this study. Pectin is unlikely to be in leaf extracts in terms of the viscosity value. Consequently, pectin seems not to be the main material which forms a black precipitate with iron ions. Furthermore, the friction reducing layer, which is mainly composed of iron and oxide, is not the first candidate for low friction; the RS result showed that graphite-like carbon was present on the BP surface, and the graphitic carbon layer is more appropriate to be the main cause of low friction.

There are several hypotheses other than these, which have been developed by the authors: bulk leaf, adhered leaf film and pectin gel. As described in Section 3.2.3, the hypothesis "bulk leaf" is likely but "pectin gel" is unlikely. The hypothesis "adhered leaf film" has not yet been examined due to the difficulty to create a leaf film on a flat steel plate; hence this hypothesis would be tested with a twin disc machine, which has been proven to be able to create a leaf film on its specimen.[11,21] This examination should be the next step.

4.2 Literature review of a chemical reaction

In this study, organics in leaf extracts were found to involve the chemical reaction with dissolved iron ions, and they might be sugars or acids which can form a chelate structure with Fe ions as summarised in Table S2.† Hence, literature was reviewed to find a possible theory of a chemical reaction process between organics and iron.

RS revealed that sugar in LEs is one of the factors which induce the chemical reaction. Based on this information, the Maillard reaction could be the most realistic candidate for the black material formation. The Maillard reaction is caused by reducing sugars and amino acids, and odorous brown pigments, called melanoidin, are generally produced after the reaction.[61,62] Both GBP and BBP have a strong and honey-like smell, especially after the boiling process. Furthermore, nitrogen was detected in XPS analysis with the chemical shift of organic matrix containing nitrogen, which might come from amino acids dissolved into LEs.

Reducing sugars, such as glucose and fructose, have been detected in tea, as well as amino acids, such as glutamine and threonine.[31,63,64] LEs used in this study are practically a cup of sycamore tea; therefore, the Maillard reaction could happen in terms of materials. Furthermore, iron and iron oxide have been reported to promote the Maillard reaction.[65,66] Additionally, melanoidin is known to have antioxidant activity;[61] melanoidin can catch metal ions, possibly forming a chelate structure with them.[67–69] It is also noteworthy that charred meats made by barbecue, which are typical melanoidin, have been reported to contain graphene oxide and nanocarbon particles.[70] These facts seem to have a close linkage to the findings in this study: sugar-derived carbon in RS, a chelate structure of iron carboxylate in FT-IR and a graphene oxide in XPS. In fact, the FT-IR spectrum of Maillard reaction products presented in[61] has a very similar absorption band: 3411, 1635, 1404 and 1076 cm^{-1}.

Another possibility to produce a black pigment with organics and irons is iron-based ink, such as iron-gall ink.[71–74] Although the chemical reaction process has not yet been elucidated, black pigments can be made with irons and tannin-derived polyphenolic materials, such as gallic acids, ellagic acids and catechin derivatives. They have been detected in tea as a water-soluble material,[31,64,75] and also they can form a chelate structure with iron oxides,[76–78] which shows a good agreement with the results in this study. Moreover, the FT-IR spectrum of the laboratory-made iron gall ink shows similar absorption patterns (1640, 1424 and 1083 cm^{-1}).[72] Furthermore, the RS spectra of iron gall ink and historical ink sample also exhibit similar Raman shifts: 1475, 1310 and broad 640–490 cm^{-1} in ref. 74 and 1590, 1315 and 1006 cm^{-1} ($CaSO_4$, detected in XRD and XPS analysis) in ref. 71.

It could be possible to suppose that organic acids simply form a chelate structure with dissolved iron ions, and then a further chemical reaction occurs on its surface. For example,

oxalate or malate can be found in plant leaf extracts,[63,79] and ferric oxalate or iron malate could be formed in LEs. Alternatively, iron ions might be able to react with gluconic acids[49] or form an iron–sugar complex.[80,81]

To sum up, three candidates that can explain the chemical reaction process are proposed through the literature review: Maillard reaction, iron-based ink and organic acid.

4.3 Possible chemical reaction process

A chemical reaction process is supposed as shown in Fig. 12. As revealed in XRF analysis, Fe ions are dissolved into LEs, possibly with the help of organic acids. Then, the dissolved Fe ions form a chelate structure with the acids, *e.g.* carboxylic acids, tannic acids and other organic acids in LEs, as suggested in FT-IR analysis. Subsequently, Fe ions are wrapped with organic molecules such as reducing sugars and amino acids. At step four, a chemical reaction occurs with organics on the surface of Fe ions, forming a carbon layer on the surface; it could be the Maillard reaction or formation of iron-gall ink. The process one to five can be applied to other dissolved Fe ions, and finally, black precipitation is formed with a three-layer structure: carbon layer on the surface, chelate layer in the middle and Fe ion as a core.

It should be noted that this process is a suggestion based on the information from the material analysis of the black materials synthesised in this study. In the actual wheel/rail contact, high pressure applied to leaves could affect the chemical reaction process, as well as high temperature induced by sliding in the wheel/rail contact.[4] To examine the proposed chemical reaction process, further experiments and analyses are necessary: identification of key organics in leaf extracts and comparison between a laboratory-developed black material and a blackened leaf film seen on the actual railway tracks.

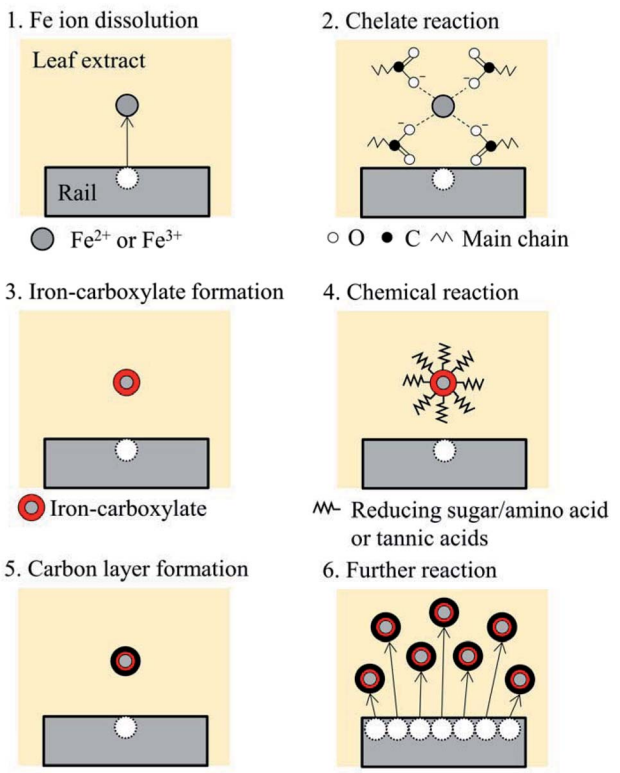

Fig. 12 Supposed chemical reaction process.

5. Conclusions

In this study, the low friction mechanism due to leaf contamination on railway tracks was investigated through pin-on-flat tests and material analyses, as well as the chemical reaction process between leaf organics and rail steels. Three types of leaf-related sample were tested: sycamore leaf powder, leaf extract and black material, which was synthesised with leaf extracts and rail steels. The black material formed in brown leaf extracts exhibited extremely low friction for 6 minutes, which is similar to that of the commercial engine oil. The leaf powder also lowered the friction level for the first 1 minute; however, the leaf extract did not show low friction. Material analyses were intensively conducted for the black material, using five techniques: X-ray fluorescence, X-ray diffraction, laser Raman spectroscopy, X-ray photoelectron spectroscopy and Fourier transform infrared spectroscopy. These analyses revealed that dissolved iron ions in leaf extracts react with organics, such as reducing sugars, amino acids and tannic acids, possibly forming a chelate structure. Then, the graphitic carbon layer is formed on the formed iron carboxylates or iron oxides with a small amount of KCl, $CaSO_4$ and phosphate compounds. This carbon material is seemingly a result of the Maillard reaction or iron-gall ink formation. Therefore, the low friction was concluded to be caused by four factors: firstly graphitic carbon, secondly bulk leaves, thirdly iron oxides, and finally phosphate compounds in the black material. The chemical reaction process was proposed; however, further experiments and analyses are necessary to examine this proposal.

Conflicts of interest

There are no conflicts to declare.

Acknowledgements

Authors gratefully acknowledge the financial support from East Japan Railway Company and Railway Safety and Standard Board. We would also like to thank Mr Robert J Hanson at the Department of Chemistry, University of Sheffield, for his assistance with the FT-IR analysis, and Mr Anup Chalisey at Railway Safety and Standards Board, for comments that greatly improved the manuscript of this proceedings.

Reference

1 C. R. Fulford, *Review of low adhesion research*, Report published by the Railways Safety and Standards Board, 2004 (May).

2 W. Poole, *Characteristics of Railhead Leaf Contamination*, Report published by the Railways Safety and Standards Board, 2007.
3 T. Pearce and D. Watkins. *Adhesion and leaves - A review of the problem and potential solutions*, Report published by the British Railways, 1987.
4 K. Ishizaka, S. R. Lewis and R. Lewis. The low adhesion problem due to leaf contamination in the wheel/rail contact: Bonding and low adhesion mechanisms. *Wear*. 2017**378–379**:183–197.
5 Rail Accident Investigation Branch, Station overrun at Stonegate, East Sussex, 8 November 2010, 2011.
6 Rail Accident Investigation Branch, Buffer stop collision at Chester station, 20 November 2013, 2014.
7 C. Morrison, Trains are being cancelled because of leaves on the tracks, City AM, 2017, Available from: http://www.cityam.com/273836/trains-being-cancelled-because-leaves-tracks.
8 A. Bagdi, Leaves on the line will force revised London Midland autumn timetable, Express & Star, 2017, Available from: https://www.expressandstar.com/news/2017/10/17/leaves-on-the-line-will-force-revised-london-midland-autumn-timetable/.
9 Z. Li, O. Arias-Cuevas, R. Lewis and E. A. Gallardo-Hernández, Rolling–Sliding Laboratory Tests of Friction Modifiers in Leaf Contaminated Wheel–Rail Contacts, *Tribol. Lett.*, 2009, **33**(2), 97–109.
10 U. Olofsson and K. Sundvall, Influence of leaf, humidity and applied lubrication on friction in the wheel-rail contact: pin-on-disc experiments, *Proceedings of the Institution of Mechanical Engineers, Part F: Journal of Rail and Rapid Transit.*, 2004, **218**(3), 235–242.
11 E. A. Gallardo-Hernandez and R. Lewis, Twin disc assessment of wheel/rail adhesion, *Wear*, 2008, **265**(9–10), 1309–1316.
12 O. Arias-Cuevas, Z. Li, R. Lewis and E. a Gallardo-Hernández, Laboratory investigation of some sanding parameters to improve the adhesion in leaf-contaminated wheel–rail contacts, *Proceedings of the Institution of Mechanical Engineers, Part F: Journal of Rail and Rapid Transit.*, 2010, **224**(3), 139–157.
13 M. Omasta, M. Machatka, D. Smejkal, M. Hartl and I. Křupka, Influence of sanding parameters on adhesion recovery in contaminated wheel–rail contact, *Wear*, 2015, **322–323**, 218–225.
14 O. Arias-Cuevas, Z. Li and R. Lewis, A laboratory investigation on the influence of the particle size and slip during sanding on the adhesion and wear in the wheel-rail contact, *Wear*, 2011, **271**(1–2), 14–24, DOI: 10.1016/j.wear.2010.10.050.
15 R. Lewis and R. S. Dwyer-Joyce, Wear at the wheel/rail interface when sanding is used to increase adhesion, *Proceedings of the Institution of Mechanical Engineers, Part F: Journal of Rail and Rapid Transit.*, 2006, **220**(1), 29–41.
16 G. Vasić, F. Franklin, A. Kapoor and V. Lučanin, Laboratory simulation of low adhesion leaf film on rail steel, *Int. J. Surf. Sci. Eng.*, 2008, **2**, 84–97.
17 P. M. Cann, The "leaves on the line" problem - A study of leaf residue film formation and lubricity under laboratory test conditions, *Tribol. Lett.*, 2006, **24**(2), 151–158.
18 Y. Zhu, U. Olofsson and R. Nilsson, A field test study of leaf contamination on railhead surfaces, *Proceedings of the Institution of Mechanical Engineers, Part F: Journal of Rail and Rapid Transit.*, 2014, **228**(1), 71–84.
19 J. W. G. Edgley, *Managing Low Adhesion*, Report published by Rail Delivery Group, 2018. Available from: https://www.raildeliverygroup.com/component/arkhive/?task=file.download&id=469773735.
20 O. Arias-Cuevas, Z. Li, R. Lewis and E. a. Gallardo-Hernández, Rolling-sliding laboratory tests of friction modifiers in dry and wet wheel-rail contacts, *Wear*, 2010, **268**(2–3), 543–551.
21 S. R. Lewis, R. Lewis, J. Cotter, X. Lu and D. T. Eadie, A new method for the assessment of traction enhancers and the generation of organic layers in a twin-disc machine, *Wear*, 2016, **366–367**, 258–267.
22 A. Synytsya, Fourier transform Raman and infrared spectroscopy of pectins, *Carbohydr. Polym.*, 2003, **54**(1), 97–106. Available from: http://www.sciencedirect.com/science/article/pii/S0144861703001589.
23 F. Tuinstra and J. L. Koenig, Raman Spectrum of Graphite, *J. Chem. Phys.*, 1970, **53**(3), 1126–1130. Available from: http://aip.scitation.org/doi/10.1063/1.1674108.
24 F. Guo, Y. Tian, Y. Liu and Y. Wang, Tribological behaviors of graphite sliding against cemented carbide in CaCl2 solution, *Surf. Topogr.: Metrol. Prop.*, 2015, **3**(4), 044003.
25 M. Saravanan, M. Ganesan and S. Ambalavanan, An in situ generated carbon as integrated conductive additive for hierarchical negative plate of lead-acid battery, *J. Power Sources*, 2014, **251**, 20–29, DOI: 10.1016/j.jpowsour.2013.10.143.
26 D. L. a. de Faria, S. V. Silva and M. T. de Oliveira, Raman microspectroscopy of some iron oxides and oxyhydroxides, *J. Raman Spectrosc.*, 1997, **28**(February), 873–878.
27 D. Lin-Vien, N. B. Colthup, W. G. Fateley and J. G. Grasselli, *The handbook of infrared and Raman characteristic frequencies of organic molecules*, Academic Press, London, 1991.
28 J. Ma, T. Xue and X. Qin, Sugar-derived carbon/graphene composite materials as electrodes for supercapacitors, *Electrochim. Acta*, 2014, **115**, 566–572, DOI: 10.1016/j.electacta.2013.11.028.
29 V. Sridhar and H. Park, Sugar-derived disordered carbon nano-sheets as high-performance electrodes in sodium-ion batteries, *New J. Chem.*, 2017, **41**(11), 4286–4290. Available from: http://xlink.rsc.org/?DOI=C6NJ03917K.
30 A. C. Ferrari and J. Robertson, Interpretation of Raman spectra of disordered and amorphous carbon, *Phys. Rev. B: Condens. Matter Mater. Phys.*, 2000, **61**(20), 95–107.
31 Y. Yuan, Y. Song, W. Jing, Y. Wang, X. Yang and D. Liu, Simultaneous determination of caffeine, gallic acid, theanine, (−)-epigallocatechin and (−)-epigallocatechin-3-gallate in green tea using quantitative 1H-NMR spectroscopy, *Anal. Methods*, 2014, **6**(3), 907–914. Available

from: http://pubs.rsc.org/en/content/articlehtml/2014/ay/c3ay41369a.

32 T. Nakahara, K. S. Baek, H. Chen and M. Ishida, Relationship between surface oxide layer and transient traction characteristics for two steel rollers under unlubricated and water lubricated conditions, *Wear*, 2011, **271**(1–2), 25–31, DOI: 10.1016/j.wear.2010.10.030.

33 D. Wiebodt, Understanding Raman Spectrometer Parameters, *Spectroscopy*, 2010, (Special Issues June). Available from: http://www.spectroscopyonline.com/understanding-raman-spectrometer-parameters?id=&sk=&date=&pageID=5.

34 N. J. Everall, J. Lumsdon and D. J. Christopher, The Effect of Laser-Induced Heating Upon the Vibrational Raman-Spectra of Graphites and Carbon-Fibers, *Carbon*, 1991, **29**(2), 133–137.

35 Thermo Scientific X-ray Photoelectron Spectroscopy XPS. Available from: http://xpssimplified.com/.

36 J. F. Moulder, W. F. Stickle, P. E. Sobol and K. D. Bomben, *Handbook of X-ray Photoelectron Spectroscopy*, ed. J. Chastain, Perkin-Elmer Corporation, Physical Electronics Division, Minnesota, 1992.

37 P. M. A. Sherwood, Introduction to Studies of Phosphorus-Oxygen Compounds by XPS, *Surf. Sci. Spectra*, 2002, **9**(1), 62–66. Available from: http://avs.scitation.org/doi/10.1116/11.20030101.

38 D. Yang, A. Velamakanni, G. Bozoklu, S. Park, M. Stoller, R. D. Piner, *et al.*, Chemical analysis of graphene oxide films after heat and chemical treatments by X-ray photoelectron and Micro-Raman spectroscopy, *Carbon*, 2009, **47**(1), 145–152.

39 D. Briggs, *Surface analysis of polymers by XPS and static SIMS*, Cambridge University Press, New York, 1998.

40 M. Barathi, A. S. Krishna Kumar, C. U. Kumar and N. Rajesh, Graphene oxide-aluminium oxyhydroxide interaction and its application for the effective adsorption of fluoride, *RSC Adv.*, 2014, **4**(96), 53711–53721.

41 B. D. Ossonon and D. Bélanger, Synthesis and characterization of sulfophenyl-functionalized reduced graphene oxide sheets, *RSC Adv.*, 2017, **7**(44), 27224–27234. Available from: http://xlink.rsc.org/?DOI=C6RA28311J.

42 L. Madec, R. Petibon, J. Xia, J.-P. Sun, I. G. Hill and J. R. Dahn, Understanding the Role of Prop-1-ene-1,3-Sultone and Vinylene Carbonate in LiNi $_{1/3}$ Mn $_{1/3}$ Co $_{1/3}$ O $_{2}$/Graphite Pouch Cells: Electrochemical, GC-MS and XPS Analysis, *J. Electrochem. Soc.*, 2015, **162**(14), A2635–A2645. Available from: http://jes.ecsdl.org/lookup/doi/10.1149/2.0741512jes.

43 T. Yamashita and P. Hayes, Analysis of XPS spectra of Fe^{2+} and Fe^{3+} ions in oxide materials, *Appl. Surf. Sci.*, 2008, **254**(8), 2441–2449.

44 A. P. Grosvenor, B. A. Kobe, M. C. Biesinger and N. S. McIntyre, Investigation of multiplet splitting of Fe 2p XPS spectra and bonding in iron compounds, *Surf. Interface Anal.*, 2004, **36**(12), 1564–1574.

45 NIST X-ray Photoelectron Spectroscopy Database. Available from: https://srdata.nist.gov/xps/.

46 B. Demri and D. Muster, XPS study of some calcium compounds, *J. Mater. Process. Technol.*, 1995, **55**(3–4), 311–314. Available from: http://www.sciencedirect.com/science/article/pii/0924013695020233.

47 D. R. Dreyer, S. Park, C. W. Bielawski and R. S. Ruoff, The chemistry of graphite oxide, *Chem. Soc. Rev.*, 2010, **39**(1), 228–240. Available from: http://www.ncbi.nlm.nih.gov/pubmed/20023850.

48 D. H. Williams and I. Fleming, *Spectroscopic Methods in Organic Chemistry*, McGraw-Hill, London, 4th edn, 1989.

49 V. Nikolic, D. Ilic, L. Nikolic, L. Stanojevic, M. Cakic, A. Tacic, *et al.*, The synthesis and characterization of iron(II): Gluconate, *Savremene tehnologije*, 2014, **3**(2), 16–24. Available from: http://scindeks.ceon.rs/Article.aspx?artid=2217-97121402016N.

50 V. Otero, D. Sanches, C. Montagner, M. Vilarigues, L. Carlyle, J. A. Lopes, *et al.*, Characterisation of metal carboxylates by Raman and infrared spectroscopy in works of art, *J. Raman Spectrosc.*, 2014, **45**(11–12), 1197–1206.

51 M. C. D'Antonio, A. Wladimirsky, D. Palacios, L. Coggiola, A. C. González-Baró, E. J. Baran, *et al.*, Spectroscopic investigations of iron(II) and iron(III) oxalates, *J. Braz. Chem. Soc.*, 2009, **20**(3), 445–450.

52 E. G. Palacios, G. Juárez-López and A. J. Monhemius, Infrared spectroscopy of metal carboxylates II. Analysis of Fe(III), Ni and Zn carboxylate solutions, *Hydrometallurgy*, 2004, **72**(1–2), 139–148.

53 V. P. Shinde and P. P. Patil, Investigation on role of monomer(s) during electrochemical polymerization of aniline and its derivatives on low carbon steel by XPS, *Electrochim. Acta*, 2012, **78**, 483–494.

54 J. Williams, *Engineering Tribology*, Cambridge University Press, New York, 2004, pp. 348–380.

55 S. S. Wang and S. C. Tung, A Reaction Mechanism for Producing Low-Friction Iron Phosphate Coatings, *Tribol. Trans.*, 1991, **34**(1), 45–50.

56 B. Guan, B. A. Pochopien and D. S. Wright, The chemistry, mechanism and function of tricresyl phosphate (TCP) as an anti-wear lubrication additive, *Lubr. Sci.*, 2016, **28**(5), 257–265. Available from: http://onlinelibrary.wiley.com/doi/10.1002/ls.77/abstract.

57 M.-C. Corneci, F. Dekkiche, A.-M. Trunfio-Sfarghiu, M.-H. Meurisse, Y. Berthier and J.-P. Rieu, Tribological properties of fluid phase phospholipid bilayers, *Tribol. Int.*, 2011, **44**, 1959–1968.

58 F. Gao, P. V. Kotvis and W. T. Tysoe, The friction, mobility and transfer of tribological films: Potassium chloride and ferrous chloride on iron, *Wear*, 2004, **256**(11–12), 1005–1017.

59 P. J. John, S. V. Prasad, A. A. Voevodin and J. S. Zabinski, Calcium sulfate as a high temperature solid lubricant, *Wear*, 1998, **219**(2), 155–161.

60 P. J. John and J. S. Zabinski, Sulfate based coatings for use as high temperature lubricants, *Tribol. Lett.*, 1999, **7**, 31–37.

61 F. Zha, B. Wei, S. Chen, S. Dong, M. Zeng and Z. Liu, The Maillard reaction of a shrimp by-product protein hydrolysate: chemical changes and inhibiting effects of reactive oxygen species in human HepG2 cells, *Food Funct.*,

2015, **6**(6), 1919–1927. Available from: http://xlink.rsc.org/?DOI=C5FO00296F.

62 U. Teruyuki, The Maillard reaction in food, *J. Integr. Study Diet. Habits*, 2015, **26**(1), 11–19.

63 N. Prefecture and A. Experiment, Prediction of Japanese Green Tea Ranking by Gas Chromatography/Mass Spectrometry-Based Hydrophilic Metabolite Fingerprinting, *J. Agric. Food Chem.*, 2007, **55**, 231–236.

64 G. Le Gall, I. J. Colquhoun and M. Defernez, Metabolite Profiling Using 1H NMR Spectroscopy for Quality Assessment of Green Tea, Camellia sinensis (L.), *J. Agric. Food Chem.*, 2004, **52**(4), 692–700.

65 I. Birlouez-Aragon, V. Moreaux, M. Nicolas and C. J. Ducauze, Effect of iron and lactose supplementation of milk on the Maillard reaction and tryptophan content, *Food Addit. Contam.*, 1997, **14**(4), 381–388.

66 Y. Kato, K. Watanabe and Y. Sato, Effect of Some Metals on the Maillard Reaction of Ovalbumin, *J. Agric. Food Chem.*, 1981, **29**(3), 540–543.

67 D. T. Ramonaityte, M. Keršiene, A. Adams, K. A. Tehrani and N. D. Kimpe, The interaction of metal ions with Maillard reaction products in a lactose-glycine model system, *Food Res. Int.*, 2009, **42**(3), 331–336.

68 A. S. P. Moreira, F. M. Nunes, M. R. Domingues and M. A. Coimbra, Coffee melanoidins: structures, mechanisms of formation and potential health impacts, *Food Funct.*, 2012, **3**(9), 903–915, DOI: 10.1039/C2FO30048F.

69 A. N. Wijewickreme and D. D. Kitts, Modulation of metal-induced genotoxicity by Maillard reaction products isolated from coffee, *Food Chem. Toxicol.*, 1998, **36**(7), 543–553.

70 M. Saxena and S. Sarkar, Involuntary graphene intake with food and medicine, *RSC Adv.*, 2014, **4**(57), 30162. Available from: http://xlink.rsc.org/?DOI=C4RA04022H.

71 G. Piantanida, E. Menart, M. Bicchieri and M. Strlič, Classification of iron-based inks by means of micro-Raman spectroscopy and multivariate data analysis, *J. Raman Spectrosc.*, 2013, **44**(9), 1299–1305.

72 S. C. Boyatzis, G. Velivasaki and E. Malea, A study of the deterioration of aged parchment marked with laboratory iron gall inks using FTIR-ATR spectroscopy and micro hot table, *Heritage Sci.*, 2016, **4**(1). Available from: http://heritagesciencejournal.springeropen.com/articles/10.1186/s40494-016-0083-4.

73 M. Bicchieri, M. Monti, G. Piantanida and A. Sodo, All that is iron-ink is not always iron-gall!, *J. Raman Spectrosc.*, 2008, **39**(April), 1074–1078.

74 A. S. Lee, P. J. Mahon and D. C. Creagh, Raman analysis of iron gall inks on parchment, *Vib. Spectrosc.*, 2006, **41**(2), 170–175.

75 G. K. Poon, Analysis of catechins in tea extracts by liquid chromatography-electrospray ionization mass spectrometry, *J. Chromatogr. A*, 1998, **794**(1/2), 63–74.

76 L. Mei, L. Liao, Z. Wang and C. Xu, Interactions between Phosphoric/Tannic Acid and Different Forms of FeOOH, *Adv. Mater. Sci. Eng.*, 2015, **2015**, 1–10.

77 S. Nasrazadani, The application of infrared spectroscopy to a study of phosphoric and tannic acids interactions with magnetite (Fe3O4), goethite (α-FeOOH) and lepidocrocit (γ-FeOOH), *Corros. Sci.*, 1997, **39**(l), 1845–1859.

78 B. Qian, B. Hou and M. Zheng, The inhibition effect of tannic acid on mild steel corrosion in seawater wet/dry cyclic conditions, *Corros. Sci.*, 2013, **72**, 1–9, DOI: 10.1016/j.corsci.2013.01.040.

79 T. R. I. Cataldi, G. Margiotta, A. Del Fiore and S. A. Bufo, Ionic content in plant extracts determined by ion chromatography with conductivity detection, *Phytochem. Anal.*, 2003, **14**(3), 176–183.

80 P. J. Charley, B. Sarkar, C. F. Stitt and P. Saltman, Chelation of iron by sugars, *Biochim. Biophys. Acta*, 1963, **69**, 313–321.

81 C. P. Rao and K. Geetha, Fe(III) complexes of D-glucose and D-fructose, *Biometals*, 1994, **7**(1), 25–29.